J Mater Sci (2010) 45:5177–5190
DOI 10.1007/s10853-010-4555-8

Perfect wettability of carbon by liquid aluminum achieved by a multifunctional flux

P. Baumli · J. Sytchev · G. Kaptay

Received: 31 January 2010 / Accepted: 16 April 2010 / Published online: 11 May 2010

Abstract The wettability of carbon (graphite and glassy carbon) by liquid aluminum was studied. A special molten salt (flux) system was developed under which perfect wettability (a zero contact angle) of liquid aluminum was achieved on carbon surfaces. The principal component of the flux is K_2TiF_6 dissolved in a molten alkali chloride. K_2TiF_6 is a multifunctional flux component as it performs the following tasks: (i) dissolves the oxide layer covering liquid aluminum, (ii) through an exchange reaction with liquid aluminum it ensures the necessary amount of Ti dissolved in liquid Al, which is needed to cover the Al/C interface by TiC. As TiC is a metallic carbide, it is perfectly wetted by liquid Al–Ti alloys. In this paper, the conditions of perfect wettability of carbon by liquid Al under MCl–K_2TiF_6 molten salts (fluxes) are found as function of: (i) the basic component of the flux (MCl = LiCl, or NaCl–KCl or CsCl), (ii) K_2TiF_6 content of the flux, (iii) temperature, (iv) flux:Al weight ratio, (v) specific surface area of Al, and (vi) specific surface area of carbon. A simplified theoretical equation is derived to reproduce the experimental data.

P. Baumli
Institute of Chemistry, University of Miskolc, Egyetemvaros, Miskolc 3515, Hungary

P. Baumli · J. Sytchev · G. Kaptay (✉)
Department of Nanocomposites, BAY-NANO Research Institute, Egyetemvaros, Miskolc 3515, Hungary
e-mail: kaptay@hotmail.com

G. Kaptay
Department of Nanotechnology, University of Miskolc, Egyetemvaros, E/7, Miskolc 3515, Hungary

Introduction

Wettability of solids by liquid metals is a subject of high importance both for theory and practice [1–13], especially for producing composite materials [14–16], metallic foams, and emulsions [1, 2, 9, 11, 17, 18]. Different forms of carbon (carbon fibers, carbon nanotubes, etc.) are among the most interesting materials due to their low density and high strength. They are already used to strengthen different bulk materials, such as polymers, ceramics, and metallic alloys. Among the metallic matrices for metal matrix composites one of the most promising is aluminum and its alloys due to their low density and good corrosion resistance. Thus, one of the interesting reinforcement/matrix compositions is the family of C/Al composites [19–35]. However, the development of C-reinforced Al-matrix composites and nanocomposites is seriously limited by the poor wettability between all forms of carbon and liquid aluminum.

Indeed, the contact angle in the graphite/liquid Al system was found between 140° and 160° at 700 °C due to the oxide layer covering liquid Al [36–41]. One of the ways to remove the oxide layer is to apply high temperature and high vacuum at the same time. Indeed, in high vacuum at a temperature of around 1000 °C the contact angle gradually reduces into the interval between 50° and 70° [36–43]. Under this condition, an Al_4C_3 layer with a thickness of 1–20 μm forms at the Al/C interface and the improved wettability corresponds rather to the Al/Al_4C_3 couple [36] and not to the original Al/C couple. However, neither high temperature nor high vacuum is desirable for materials processing. Moreover, the interfacial wettable product (Al_4C_3) is a forbidden component of Al-matrix composites due to its corrosion sensitivity.

The formation of Al_4C_3 can be reduced or eliminated by alloying liquid aluminum with elements forming more

stable carbides compared to Al. These attempts were successful with Si [40, 44] and Ti [40] alloying. However, perfect wettability (a zero contact angle) has not been reported in these experiments [40, 41, 44].

Wettability of carbon by liquid Al can be improved by coating the carbon surface by metals or metal-like ceramics [45]. Among metals Ni [23, 46], Cu [47], and Ti [39], while among the metal-like ceramics TiB_2 [21, 39] was successfully applied.

Molten salts (fluxes) are frequently used in processing Al-alloys, mostly to remove their oxide layers and to remove the oxide inclusions from aluminum [48, 49]. Wettability of carbon by different Al-alloys was also studied under protective fluxes [50, 51]. Pure liquid Al covered by eutectic $KAlF_4$–K_3AlF_6 flux was found to have poor wettability on graphite particles at 800 °C [51]. On the other hand, it was found that liquid Al alloyed with 5 wt% of Ti, Hf, V, Nb, Ta, and Mg perfectly wets a graphite surface under the protective NaCl–KCl flux at temperatures above 900 °C [50].

In some studies on the behavior of Al–Ti and Al–Ti–B alloys under KF–AlF_3 and cryolite–alumina melts, perfect wettability of the graphite crucible by the liquid alloy was found [52–54]. However, these findings were side-products (to be eliminated) in those studies, and were not studied systematically.

The goal of this paper is to report on our systematic studies to achieve perfect wettability of graphite and glassy carbon surfaces by liquid Al under a molten salt (flux).

Our concept to achieve perfect wettability of graphite by liquid Al

First, let us develop a concept to make graphite surfaces perfectly wettable by pure liquid Al, using a molten salt flux. From the above literature review, this flux should be at least bi-functional, as it should:

(i) remove the oxide layer from the surface of liquid Al and protect liquid Al from further oxidation, and
(ii) provide in situ alloying of liquid Al by a component which will ensure perfect wettability of graphite by this alloy.

The removal of oxide layer is routinely achieved by chloro-fluoride fluxes, namely by equimolar NaCl–KCl with some dissolved fluorides such as KF [48, 49], AlF_3, MgF_2, CaF_2, NaF, LiF, Na_3AlF_6 [49]. Thus, in this paper equimolar NaCl–KCl salt will also be used with some fluoride additives.

Now, let us select the alloying element for Al. As follows from some observations in the literature, transition metals being able to produce stable carbides of metallic character can improve the wettability of Al on graphite [50]. Titanium will be selected in this paper as it has been proven an efficient alloying component to enhance wettability in many systems [41]. Also, some literature observations indicate that perfect wettability in the Al–Ti/C system can be achieved under some molten salts [50, 52–54].

At the Al–Ti/C interface, the formation of TiC is thermodynamically expected [55–60]. Although TiC is not perfectly wetted by liquid Al in a gas atmosphere [41, 61–63], it was found perfectly wettable under the AlF_3–KF eutectic [51, 60, 64].

It has been known for some decades that one of the economical ways to produce Al–Ti and Al–Ti–B alloys is reacting liquid Al with a K_2TiF_6-containing molten salt [65–69]. Moreover, the formation of in situ Al/TiC composites were reported by reacting liquid Al with K_2TiF_6 and graphite particles [70], indicating the possibility to produce metallic TiC layer on graphite using Al and K_2TiF_6. Although we have found no experimental information on the ability of K_2TiF_6 to remove the oxide layer from liquid Al, from the tendency reported in [49], one can suppose that K_2TiF_6 is probably an efficient salt to do this job.

Based on the above, the molten salt system NaCl–KCl–K_2TiF_6 has been selected for this study. It has been supposed that this salt will be able to meet both the requirements mentioned above. To support this hypothesis and to help to design the experiments, a series of preliminary theoretical studies were performed (see Appendices 1–7).

Experimental conditions

The experiments were performed in glassy carbon and graphite crucibles. It was empirically established that no significant difference in wettability can be found between these two types of crucibles (a similar conclusion was made for the wettability of graphite and glassy carbon by different molten chlorides [71]). Due to economic considerations, the majority of experiments were performed in graphite crucibles. These crucibles were cylinders of 17 mm inner diameter and 30 mm height.

The weighed amounts of Al and salt were placed into a crucible. Aluminum was added in one piece of a cube-like shape, while the salt was added as powder of 0.1 mm average particle size. The crucible was placed into a stainless steel container (with a volume of about 1 L) and the latter was sealed. The container was filled with argon gas with the residual oxygen and water total partial pressure estimated to be 1 Pa. The system was heated to the desired temperature and kept at this temperature during 1 h. Then, the container was taken out of the furnace and

left to cool down to room temperature. Solidification of the alloy and the flux took about 10 min. The flux was dissolved from the room temperature crucible using water. After dissolution of the flux, the Al-droplet was removed from the crucible. Contact angle was found from the photographs of the solidified droplet. In some cases (especially in case of perfect wettability), the Al-droplet could not be removed from the crucible. In these cases, the crucible was sectioned and the contact angle was found from the photographs of these sections.

Experimental results and discussion

Qualitative differences between the shapes of solidified Al-droplets can be seen in Fig. 1. When the flux was a simple (NaCl–KCl) equimolar solution (see Fig. 1a), the droplet was clearly nonwetting and its surface was oxidized. When some NaF was added to the salt, it was able to dissolve the oxide layer from the surface of Al (see the shiny droplet in Fig. 1b), but it did not improve the wettability much. Perfect wettability was achieved when sufficient amount of K_2TiF_6 was added to the flux: see the Al-droplet climbing up the wall of the crucible against gravity in Fig. 1c. It should be mentioned that the Al droplet was able to climb up along the crucible wall only till the top of the flux layer. It stopped at the top of the flux layer probably due to different contact angle values in the carbon/Al/salt and in the carbon/Al/Ar gas systems, or perhaps due to the oxidation of Al without the protecting flux by traces of oxygen and/or water in the argon gas.

From Fig. 1c, we can conclude that our main goal is achieved and our concept to make graphite (or glassy carbon) perfectly wettable by liquid Al under a flux is proven. In the following subchapters, the influence of different parameters on wettability is reported.

Effect of K_2TiF_6 content of the flux on wettability

In Fig. 2a, the influence of K_2TiF_6 concentration of the flux on the contact angle as function of the flux to Al mass ratio (m_F/m_{Al}) is shown. For a given K_2TiF_6 content (see the curve with 10 wt% K_2TiF_6), the contact angle is about 130° in the interval of m_F/m_{Al} between zero and a certain concentration-dependent value (around 2 in case of the 10 wt% K_2TiF_6 containing flux). Then, within a limited interval of m_F/m_{Al} the contact angle gradually decreases from nonwetting (around 130°) to perfectly wetting (0°) situation. In case of the 10 wt% K_2TiF_6-containing flux, the transition from nonwetting case to the perfectly wetting case takes place in the interval of m_F/m_{Al} values between 2.0 and 3.5. With further increase of the m_F/m_{Al} ratio, the state of perfect wettability is not changed.

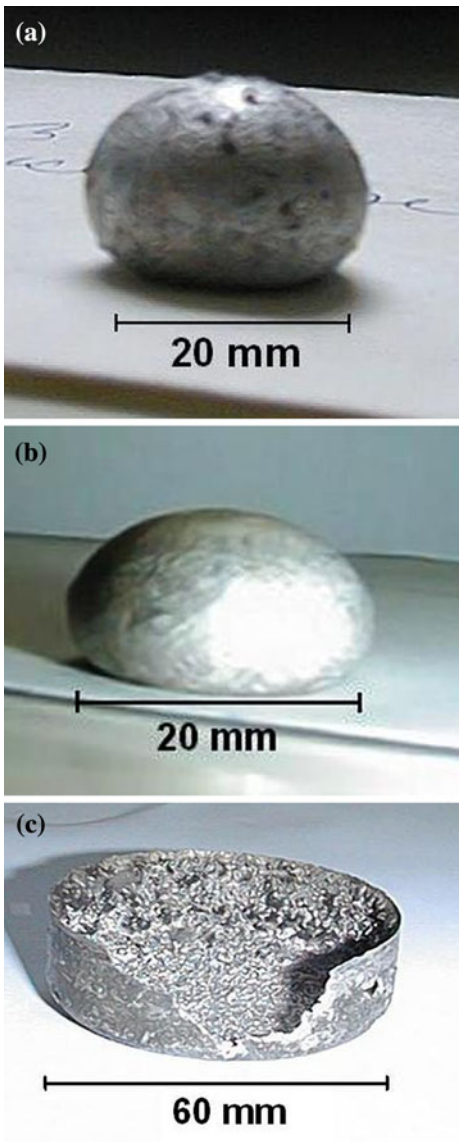

Fig. 1 Photographs of the Al-droplet taken out of glassy carbon crucibles after experiments performed at 700 °C and $m_F/m_{Al} = 8$. Flux compositions: (NaCl–KCl) (**a**), (NaCl–KCl)–10 wt% NaF (**b**), and (NaCl–KCl)–10 wt% K_2TiF_6 (**c**)

As follows from Fig. 2a, increasing the K_2TiF_6-content of the flux shifts the curves toward lower m_F/m_{Al} values. Thus, the higher is the K_2TiF_6-content of the flux, the less flux is needed for the given amount of Al to achieve perfect wettability. This is in perfect qualitative agreement with Eq. 25 of Appendix 7. To demonstrate it in a more quantitative way, Fig. 2b is plotted in coordinates dictated by Eq. 25b. One can see that the correlation is acceptable ($R^2 = 0.981$), with semi-empirical parameters: $A = 0.400$, $B = 37.2$. From Eqs. 25b–c, using parameters $m_{Al} = 3.0 \times 10^{-4}$ kg and $A_C = 4.5 \times 10^{-4}$ m^2, the values of semi-empirical parameters of Eq. 25 are found as: $k_{loss} = 2.4 \times 10^{-7}$, $k_{ox} = 4.7 \times 10^{-3}$. The latter value has

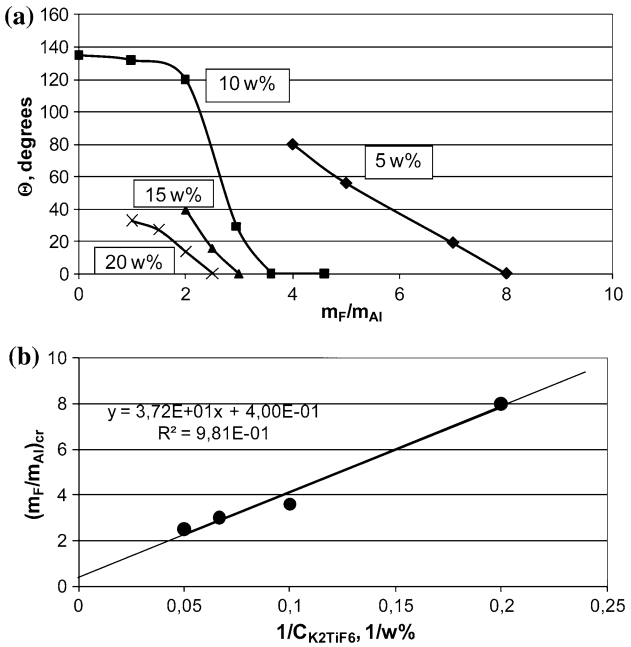

Fig. 2 Influence of K_2TiF_6 concentration of the flux (see numbers on curves in **a**) on the contact angle of liquid Al on graphite in the (NaCl–KCl)–K_2TiF_6 system as function of the mass ratio of flux to Al ($m_{Al} = 0.3$ g, $A_C = 450$ mm^2, $T = 800$ °C) (dot size corresponds to experimental uncertainty). **b** The plot in accordance with Eq. 25a of Appendix 7

the same magnitude as estimated in Appendix 7 ($k_{ox} = 2.7 \times 10^{-3}$). These parameters are approximately valid for the (NaCl–KCl) molten salt, at $T = 800$ °C.

Effect of temperature on wettability

In Fig. 3, the effect of temperature on wettability as function of m_F/m_{Al} is shown. One can see that at lower temperatures more salt is needed for the same weight of Al to ensure perfect wettability. The curves are shifted to higher m_F/m_{Al} values much more when T is decreased from 800 to 700 °C as compared to when T is decreased from 900 to 800 °C. This is in agreement with our theoretical prediction shown in Fig. 11, with the calculated critical temperature of TiC formation of around 750 °C. That is why perfect wettability at 700 °C can be achieved only due to the overheating effect of the exchange reaction (2) (see Appendix 1). Thus, an extra amount of K_2TiF_6 should have been reacted for this purpose, explaining the significantly higher values of m_F/m_{Al} required for perfect wettability at 700 °C.

The effect of temperature between 800 and 900 °C cannot be explained by Fig. 11. This effect is explained by the T-dependence of parameter k_{ox} of Eq. 25. Indeed, the definition of $k_{ox}\left(\equiv 2740 \times \frac{\delta_{ox}}{C^*}\right)$ involves the solubility of alumina in pure K_2TiF_6 (C^*). It is obvious that C^* increases with temperature [76], and thus k_{ox} is expected to decrease with T. Thus, in accordance with Eq. 25, the m_F/m_{Al} ratio is expected to decrease with temperature, even if T is above the critical value of 750 °C. However, the effect of T is smaller above 750 °C compared to its qualitative influence below 750 °C.

Effect of NaF-content of the flux on wettability

In Fig. 4, the effect of NaF-content of the flux on wettability is shown as function of m_F/m_{Al}. In these experiments, 10 wt% NaF was added to the "standard" flux of NaCl–KCl–10 wt% K_2TiF_6. As follows from Fig. 4, the addition of NaF lowered the critical m_F/m_{Al} value needed for perfect wettability. As follows from Fig. 1b, NaF itself does not ensure improved wettability. However, it is able to dissolve the oxide layer from the surface of the Al droplet, and in this way decreases the amount of Ti needed to achieve perfect wettability. In terms of Eq. 25, the role of NaF is equivalent to making coefficient k_{ox} equal to zero, i.e., no

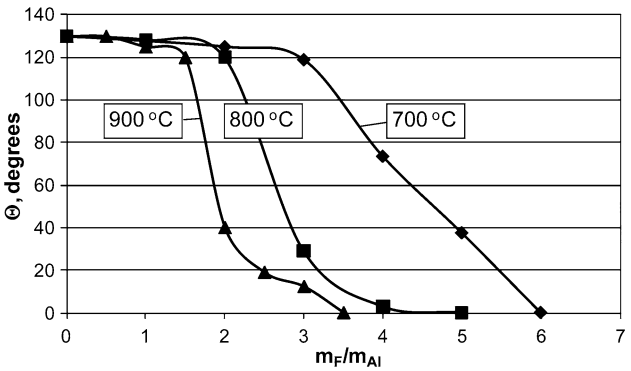

Fig. 3 Influence of temperature (see values on curves) on the contact angle of liquid Al on graphite in the (NaCl–KCl)–10 wt% K_2TiF_6 system as function of the mass ratio of flux to Al ($m_{Al} = 0.3$ g, $A_C = 450$ mm^2) (dot size corresponds to experimental uncertainty)

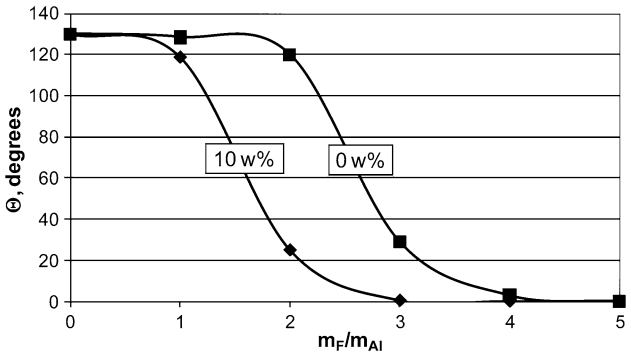

Fig. 4 Influence of NaF-content of the flux (see values on curves) on the contact angle of liquid Al on graphite in the (NaCl–KCl)–10 wt% K_2TiF_6 system as function of the mass ratio of flux to Al ($m_{Al} = 0.3$ g, $A_C = 450$ mm^2, $T = 800$ °C) (dot size corresponds to experimental uncertainty)

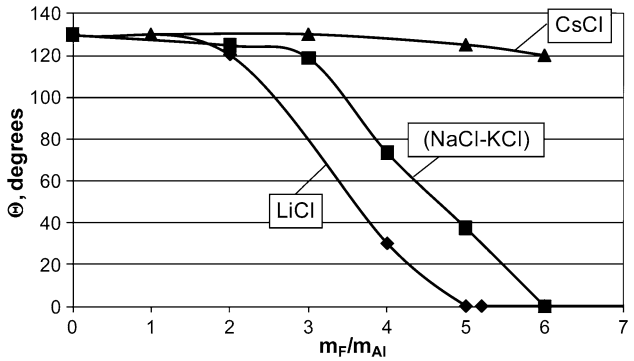

Fig. 5 Influence of the choice of alkali chlorides MCl (see on *curves*) on the contact angle of liquid Al on graphite in the MCl–10 wt% K_2TiF_6 system as function of the mass ratio of flux to Al ($m_{Al} = 0.3$ g, $A_C = 450$ mm^2, $T = 800$ °C) (dot size corresponds to experimental uncertainty)

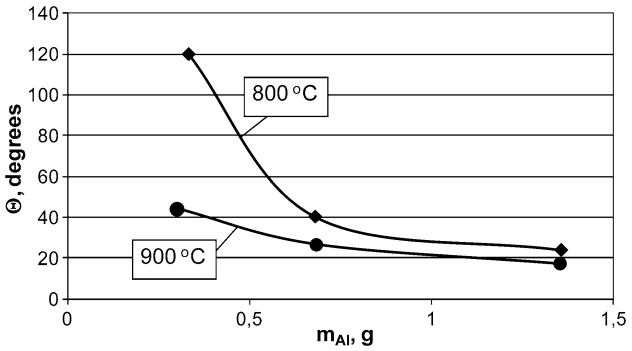

Fig. 6 Dependence of the contact angle of liquid Al on graphite on the mass of the Al droplet in (NaCl–KCl)–10 wt% K_2TiF_6 flux at two different temperatures (see values on curves, $A_C = 450$ mm^2, mass ratio of flux to Al equals 2, dot size corresponds to experimental uncertainty)

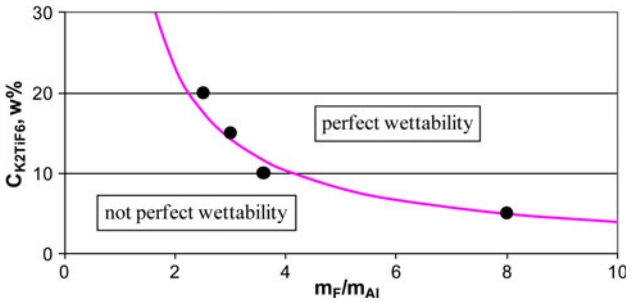

Fig. 7 The wettability diagram of graphite by liquid Al in the C/Al/(NaCl–KCl)–K_2TiF_6 system at 800 °C ($m_{Al} = 0.3$ g, $A_C = 450$ mm^2). *Points*: experimental data (see Fig. 2a), *line*: calculated by Eq 25a with parameters: $A = 0.400$, $B = 37.2$ found from Fig. 2b (dot size corresponds to experimental uncertainty)

Ti is needed to dissolve the oxide layer in the presence of NaF. As 10 wt% NaF fully dissolves the oxide layer, further increase in NaF concentration has no additional effect on wettability.

Effect of the choice of alkali chlorides on wettability

In addition to equimolar (NaCl–KCl) flux, there are other possible alkali chlorides which can in principle provide a similar function. In Fig. 5, the wettability of *C* by Al is compared depending on the choice of the alkali chloride. One can see that the wettability improved by replacing (NaCl–KCl) by LiCl, while replacing (NaCl–KCl) by CsCl made liquid Al much less wetting. This is explained by different complexing abilities of alkali chlorides toward transition metal fluorides. It is known [72] that by increasing the radius of the alkali metal cation (M) the complexing ability increases. This means that in the CsCl environment the activity of K_2TiF_6 is seriously reduced as compared to (NaCl–KCl) and especially to LiCl. Thus, the solubility of alumina in the CsCl–K_2TiF_6 salt is obviously much lower compared to (NaCl–KCl)–K_2TiF_6 and especially to LiCl–K_2TiF_6 salts, and that is why the k_{ox} value in Eq. 25 becomes much higher in the case of CsCl–K_2TiF_6. This explains why wettability cannot be improved in the CsCl–K_2TiF_6 flux.

Effect of the mass of Al droplet on wettability

When the mass of Al-droplet is small (below 1 g), it has a very high-specific surface area and that is why the amount of oxide carried with it into the system is significantly increased. The influence of the mass of the Al sample can be seen in Fig. 6. One can see that in the transition period between the nonwetting and perfectly wetting states, the mass of Al sample has a significant influence on the contact angle when it is below 1 g. This is in full accordance with Eq. 25.

The wettability diagram

As a summary to this chapter, a "wettability diagram" is shown in Fig. 7 for the (NaCl–KCl)–K_2TiF_6 system and parameters $T = 800$ °C, $m_{Al} = 0.3$ g, $A_c = 450$ mm^2. Figure 7 follows from Fig. 2a and b. One can see that Fig. 7 is in a good agreement with Eq. 25 and the model developed in Appendix 7.

Conclusions

(i) A new concept has been presented to make graphite (and glassy carbon) surfaces perfectly wettable by liquid aluminum. This implies covering liquid Al by a NaCl–KCl–K_2TiF_6 molten flux, preferably above 750 °C. The key component of the flux, K_2TiF_6, dissolves the oxide layer from the surface of liquid Al and provides the Ti-source to alloy Al by an

exchange reaction with it. The titanium being dissolved in Al interacts with carbon to form TiC above 750 °C and a Ti-content of 0.40 wt%. Liquid Al–Ti alloy perfectly wets this metallic carbide.

(ii) Perfect wettability of glassy carbon and graphite was experimentally achieved by liquid Al under different MCl–K_2TiF_6 molten flux systems as function of K_2TiF_6-content of the flux, temperature, alkali chloride (MCl), the weight of Al sample and the NaF-content of the flux. The wettability was found to improve with increasing the flux-to-Al ratio, the K_2TiF_6 content of the flux, temperature, NaF content of the flux, weight of Al and by replacing the "standard" flux MCl = (NaCl–KCl) by MCl = LiCl.

(iii) The model based on mass balance equations was developed to connect the necessary flux-to-Al mass ratio for perfect wettability with K_2TiF_6 content of the melt, mass of Al and surface area of carbon to be wetted (see Eq. 25 with two semi-empirical parameters). These parameters were found by fitting the experimental data to Eq. 25.

(iv) Finally, it should be recognized that the formation of a thin TiC-layer at the Al/C interface could not be proven by us experimentally in the course of this study. On the other hand, the macroscopic observations on perfect wettability are in full agreement with the hypothesis of the formation of this TiC-layer (see Appendices and available literature). Thus, an experimental proof of the formation of a thin TiC layer under the given experimental conditions remains an open challenge for further studies.

Acknowledgements This work was partly financed by the PhD program of the University of Miskolc and the Deák scholarship (P. Baumli) and partly by the NAP-NANO and by the CK 80255 OTKA-NKTH projects of Hungary.

Appendix 1: On the exchange reaction between the flux and liquid Al

When a NaCl–KCl–K_2TiF_6 salt comes into contact with liquid Al, the following exchange reaction is expected:

$$3(K_2TiF_6) + 4[Al] = (K_3AlF_6) + 3(KAlF_4) + 3[Ti] \quad (1)$$

with round brackets indicating that the component is dissolved in the molten salt, while square brackets indicate that the given component is dissolved in the liquid metal. As follows from the binary Al–Ti phase diagram, a very low amount of Ti dissolved in liquid Al is sufficient to reach the two-phase region (Al–Ti) + Al_3Ti [73]. Thus, Eq. 1 can be re-written in the following form, supposing that Al_3Ti particles are dispersed in the liquid Al–Ti alloy:

$$3(K_2TiF_6) + 13[Al] = (K_3AlF_6) + 3(KAlF_4) + 3\{Al_3Ti\} \quad (2)$$

The {} brackets indicate that the given pure phase is dispersed in the liquid metallic phase. Standard Gibbs energies of components are collected in Table 1 in the T-interval between 1000 and 1200 K. Most data are taken from [74]. For some components, data are missing from [74, 75] and other available sources of standard thermodynamic data. In these situations, data were estimated in this paper. In case of $KAlF_4$ for this purpose the known values for K_3AlF_6, KF, AlF_3 [74] and the information for the KF–AlF_3 phase diagram [76] were used. In case of K_2TiF_6 for this purpose the measured equilibrium vapor pressure of TiF_4 over K_2TiF_6 [77] combined with known thermodynamic data for KF and TiF_4 [74, 75] and the KF–TiF_4 phase diagram [78] were used.

The standard Gibbs energy change of reaction (2) is given in Table 2 in the same T-interval between 1000 and 1200 K. One can see that this value is very much negative (−870.0 ± 260 kJ at 1100 K), leading to very high value of the equilibrium constant of reaction (2): $K = 9 \times 10^{28} \cdots 5 \times 10^{53}$ at $T = 1100$ K. Such a high value of the equilibrium constant will guarantee that reaction (2) will be almost entirely shifted to the right hand side. In other words, all available Ti in the form of K_2TiF_6 will

Table 1 Standard Gibbs energies of formation of some compounds in the T-interval between 1000 and 1200 K ($\Delta_fG^\circ = a + b \times T$, Δ_fG° in kJ/mol, T in K)

Component	a	b	Δ_fG^o at 1100 K	Source
Al, K, C, Ti, F_2	0	0	0	By definition
K_3AlF_6	−3488.2	0.7055	−2712.2 ± 20	[74]
$KAlF_4$	−2152.5	0.40	−1712.5 ± 40	Estimated
K_2TiF_6	−3035.2	0.54	−2441.2 ± 30	Estimated
KF	−617.1	0.150	−452.1 ± 5	[74]
CF_4 (g)	−656.2	0.1135	−531.4 ± 10	[74]
Al_3Ti	−182.3	0.0615	−114.7 ± 10	[74]
TiC	−184.6	0.0115	−172.0 ± 10	[74]
Al_4C_3	−257.7	0.0945	−153.8 ± 10	[74]

Table 2 Standard Gibbs energy changes of some reactions in the T-interval between 1000 and 1200 K ($\Delta_rG^\circ = a + b \times T$, Δ_rG° in kJ, T in K)

Reaction	a	b	Δ_rG^o at 1100 K
(2)	−1387.0	0.470	−870.0 ± 260
(3)	+960.2	−0.115	+833.7 ± 60
(4)	−85.9	0.0315	−51.3 ± 3
(5)	−2.3	−0.050	−57.3 ± 20
(6)	+83.6	−0.0815	−6.1 ± 23

eventually appear in Al as dissolved Ti, or as part of the precipitated Al_3Ti intermetallic phase (see also Appendix 7).

From Table 2, one can also see that the enthalpy change of reaction (2) is about -1387 ± 200 kJ, i.e., reaction (2) is very much exothermic. According to reaction (2), 6 mol of KF, 4 mol of AlF_3, and 3 mol of Al_3Ti participate in this reaction, with the total heat capacity of about 1160 ± 50 J/K [74, 75]. Thus, one can expect that the enthalpy change of reaction (2) will heat the system maximum by $1{,}200 \pm 200$ K. In reality, only a small fraction of this T-increase will be realized in the crucible due to a larger heat capacity of the whole system (NaCl–KCl, Al, crucible) and the natural heat loss. Nevertheless, the several hundreds of K of temperature increase reported in [65] for a similar reaction seems to be supported by this simplified calculation. Thus, one can expect that the real temperature within the crucible during the experiments will be somewhat higher than the nominal temperature indicated by the thermocouple positioned at some distance from the crucible. As a side effect, one might expect the undesired formation of aluminum carbide. However, characterization of the carbon/Al–Ti interfaces was not part of this project. It is a question remaining for following studies whether aluminum carbide is formed at the interface due to the above described exothermic effect.

Appendix 2: Liquidus temperature of the flux

From the economic and environmental points of view, the temperature of the process should be kept as low as possible. Due to the melting point of Al, the process should be run at least at 700 °C or above. Thus, the selected molten salt and the molten salt resulting from reaction (2) should have a liquidus temperature below 700 °C.

The binary equimolar NaCl–KCl system forms an azeotropic solution with a liquidus/solidus temperature of about 665 °C [79]. In this paper, the equimolar NaCl–KCl solution is denoted as (NaCl–KCl). The liquidus curve in the quasi-binary (NaCl–KCl)—K_2TiF_6 system was constructed by us (see Fig. 8) from the reciprocal Na^+, K^+//TiF_6^{2-}, Cl^- system reported in [80]. One can see that more than 90 wt% of K_2TiF_6 can be dissolved in (NaCl–KCl) without increasing the liquidus temperature above 700 °C.

As it was shown above, K_2TiF_6 reacts with liquid Al forming K_3AlF_6 and $KAlF_4$ according to reaction (2). The liquidus curve in the quasi-binary (NaCl–KCl)–K_3AlF_6 system was constructed by us (see Fig. 9) from the reciprocal NaCl–KCl–K_3AlF_6–Na_3AlF_6 system reported in [81, 82]. One can see that the liquidus temperature rises above 700 °C when more than 20 wt% of K_3AlF_6 is dissolved in (NaCl–KCl).

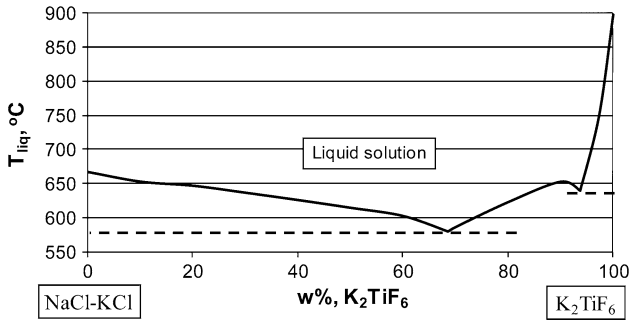

Fig. 8 Liquidus temperature in the quasi-binary (NaCl–KCl)–K_2TiF_6 system (drawn from the reciprocal Na^+, K^+//TiF_6^{2-}, Cl^- system of [80])

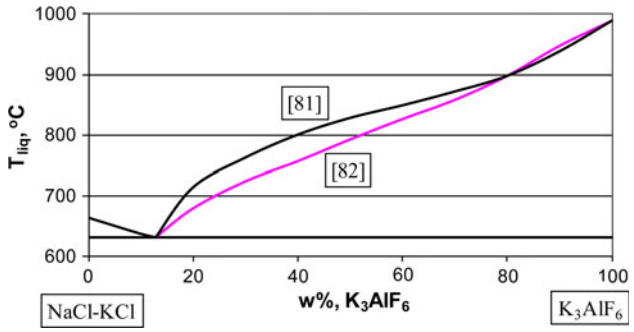

Fig. 9 Liquidus temperature in the quasi-binary (NaCl–KCl)–K_3AlF_6 system (curves are drawn from the reciprocal NaCl–KCl–K_3AlF_6–Na_3AlF_6 system. The two versions are taken from two sources [81, 82])

Unfortunately, no information on the (NaCl–KCl)–$KAlF_4$ or on the (NaCl–KCl)–K_3AlF_6–$KAlF_4$ systems was found by us in the literature. However, from the binary KF–AlF_3 phase diagram it is quite obvious that when K_3AlF_6 is replaced by the same weight of $KAlF_4$, the liquidus temperature will somewhat decrease. Thus, the liquidus curve in Fig. 9 can be considered as a maximum liquidus for the same wt% of ($KAlF_4$ + K_3AlF_6) in the (NaCl–KCl) system. As mentioned above, a maximum of 20 wt% of ($KAlF_4$ + K_3AlF_6) is allowed in the system to ensure that the liquidus temperature is kept below 700 °C. This corresponds to about 21 wt% maximum initial K_2TiF_6 content in the (NaCl–KCl) melt, in agreement with reaction (2).

In some experiments, NaF is added to (NaCl–KCl), as a less expensive substitute of K_2TiF_6 at least for the role to dissolve the oxide layer from the surface of liquid Al. The quasi-binary liquidus temperature for the (NaCl–KCl)–NaF system is shown in Fig. 10. It is constructed from ternary data of [83]. One can see that the liquidus temperature can be kept below 700 °C if the content of dissolved NaF does not reach 21 wt%.

Based on the above phase diagram information, the (NaCl–KCl) + 10 wt% K_2TiF_6 system will be used by us

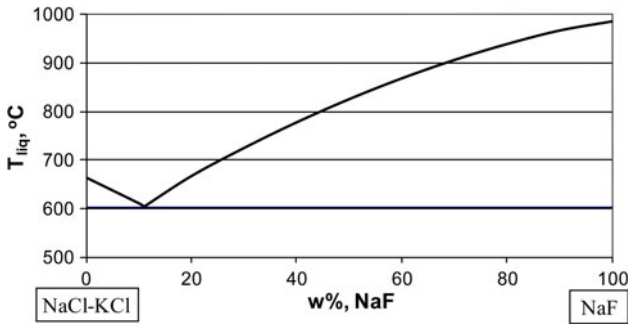

Fig. 10 Liquidus temperature in the quasi-binary (NaCl–KCl)–NaF system (drawn from the ternary NaCl–KCl–NaF system of [83])

as a "standard" flux. In some experiments, a maximum of 10 wt% of NaF will be added. All these salts will have their liquidus temperature below 700 °C with and/or without their exchange reaction with liquid Al.

Appendix 3: Density of the flux

To ensure effective phase separation between liquid Al and the covering flux, the density of the molten salt system should be kept significantly below the density of liquid Al. Density values of some pure salts are collected in Table 3. One can see that all the possible components of the salts have somewhat lower densities compared to liquid Al. In the first approximation one can suppose that the density of (NaCl–KCl)-based fluxes are linear combinations of the densities of pure components multiplied by their weight ratios. This is quite well confirmed by actual measurements [87, 88].

Then, the density of the (NaCl–KCl) + 10 wt% K_2TiF_6 flux at 1100 K will be about 1576 kg/m^3, which is lower by 32% compared to the density of liquid Al. According to reaction (2), the salt (NaCl–KCl) + 3.6 wt% K_3AlF_6 + 5.9 wt% $KAlF_4$ will form from the (NaCl–KCl) + 10 wt% K_2TiF_6 flux. The approximate density of this salt is about 1542 kg/m^3. Thus, in the course of reaction (2) the density of the salt is expected to decrease by about 2%, while the density of liquid Al is expected to increase slightly, due to alloying by heavier Ti.

Thus, we can conclude that the "standard" flux (NaCl–KCl) + 10 wt% K_2TiF_6 system with and/or without its exchange reaction with liquid Al will have a significantly lower density compared to liquid Al, i.e., the flux will form a stable liquid layer on the top of liquid Al.

Table 3 Densities of some pure liquid metals and molten salts ($\rho = a + b \cdot T$, ρ in kg/m^3, T in K)

Pure component	a	b	ρ at 1100 K	Source
Al	2707	−0.35	2322	[84]
Ti	4130	−0.23	3877	[84]
NaCl	2139.3	−0.5430	1542	[85]
KCl	2135.9	−0.5831	1494	[85]
NaF	2655	−0.54	2061	[85]
KF	2646.4	−0.6515	1930	[85]
Na_3AlF_6	3288	−0.937	2257	[76]
K_3AlF_6	3222	−1.05	2067	Estimated[a]
$NaAlF_4$	2572	−0.75	1747	[76]
$KAlF_4$	2520	−0.84	1596	Estimated[a]
K_2TiF_6	2771.5	−0.6102	2100	[86]

[a] Estimated from the values of Na_3AlF_6 and from the comparison of the NaCl–KCl and NaF–KF couples

Appendix 4: Chemical interaction between flux and graphite

In principle, TiC can be formed due to the chemical interaction of the K_2TiF_6 of the flux and graphite:

$$K_2TiF_6 + 2C = TiC + 2KF + CF_4 \quad (3)$$

As one can see from Table 2, the standard Gibbs energy change of this reaction is a highly positive value, i.e., reaction (3) in reality does not take place.[1] Thus, the graphite surface cannot be covered by TiC using the molten salt alone. The spontaneous reducing effect of liquid aluminum is needed to reduce Ti from its Ti^{+4} form (see Appendix 1). Only the reduced form of Ti is able to form the TiC layer on graphite (see below), even if its activity is lowered due to alloy formation.

Appendix 5: Thermodynamic conditions to precipitate TiC at the Al–Ti/C interface

The next condition for our successful experiments is to meet thermodynamic criteria to form TiC at the Al–Ti/C interface. Without dissolved Ti in liquid Al, the following chemical interaction is expected to take place:

[1] From Table 2, the standard Gibbs energy change of reaction (3) is +833.7 ± 60 kJ at 1100 K, with an equilibrium constant of less than 10^{-36}. Taking into account possible activities of the other components, the equilibrium vapor pressure of CF_4 will be lower than 10^{-30} bar. This reaction takes place at the graphite/molten salt interface. The vapor pressure of 10^{-30} bar is not sufficient to form a new CF_4 bubble. However, CF_4 can enter the pores of the graphite. The closed system used in our experiments is about 10^{-3} m^3 of total volume. Thus, if the law of ideal gas is supposed with the total volume occupied by the CF_4 gas, the maximum number of moles of CF_4 will be $<10^{-36}$ mol. Thus, reaction (3) will lead to the formation of less than 10^{-36} mol of TiC, being much less than a single TiC molecule.

$$4/3\mathrm{Al} + \mathrm{C} = 1/3\,\mathrm{Al_4C_3}. \quad (4)$$

As follows from Table 2, reaction (4) will take place spontaneously at any reasonable temperature with liquid Al. When the content of dissolved Ti in liquid Al is sufficient to form Al_3Ti, the following chemical reaction with graphite can also take place:

$$\mathrm{Al_3Ti} + \mathrm{C} = 3\mathrm{Al} + \mathrm{TiC} \quad (5)$$

In principle, reactions (3–5) should be analyzed together. However, due to highly positive Gibbs energy change of reaction (3), in the first approximation only reactions (4–5) will be considered here. As follows from Table 2, the standard Gibbs energy of reaction (5) is less negative at 0 K compared to reaction (4). However, at $T = 1100$ K reaction (5) is accompanied with a more negative standard Gibbs energy change compared to reaction (4). The competition between reactions (4–5) is more obvious if one considers the following exchange reaction, obtained as the difference between reactions (4) and (5):

$$1/3\,\mathrm{Al_4C_3} + \mathrm{Al_3Ti} = \mathrm{TiC} + 13/3\,\mathrm{Al} \quad (6)$$

From the Gibbs energy values given in Table 2, one can see that this reaction is improbable at low temperatures, but becomes more and more probable at higher temperatures. At a given critical temperature T_{cr}, the Gibbs energy of reaction (6) becomes zero. From the values given in Table 2, this takes place at $T_{cr} = 1026 \pm 100$ K $= 753 \pm 100$ °C. The uncertainty of this value is quite high. Unfortunately, similar uncertainties can be found in the literature (see Table 4). As follows from Table 4, T_{cr} is found between 693 and 900 °C in the literature [55–60].

The above findings are super-positioned onto the binary Al–Ti phase diagram [73] in Fig. 11. According to the dotted lines of Fig. 11, there are two thermodynamic conditions to form a stable TiC phase at the Al–Ti/C interface:

(i) temperature should be above 750 °C,
(ii) Ti-content of the remaining melt should be above a certain T-dependent value. The critical Ti-content is around $C_{Ti,cr} = 0.40$ wt% at 750 °C. This Ti-content is the coordinate of the liquidus line at 750 °C. The critical Ti-content slightly increases with increasing T. The (almost) vertical dotted line in Fig. 11 was calculated using the T-dependence of the partial excess Gibbs energy of Ti in infinitely diluted solution of liquid Al (G is in kJ/mol, T is in K):

$$\Delta G^{E\infty}_{\mathrm{Ti(Al)}} = -104.6 \exp\left(-\frac{T}{2325}\right). \quad (7)$$

Table 4 The critical (equilibrium) temperature of the nonvariant reaction (6)

T_{cr}, °C	Source	Method
<1100	[55]	Experiment
754 … 797	[56]	Experiment + calculation
<1000	[57]	Experiment
693	[58]	Calculation
<1100	[59]	Experiment
800 … 900	[60]	Experiment

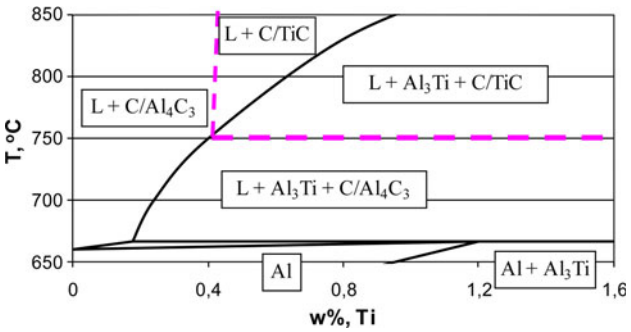

Fig. 11 The Al-corner of the binary Al–Ti phase diagram [73] with superimposed phase transition lines at the Al–Ti/C interface. *Bold lines*: equilibrium lines of the Al–Ti equilibrium phase diagram. The almost vertical *dotted line* is calculated by Eq. 9. The horizontal *dotted line* is drawn to higher Ti-contents from the point of intersection of the almost vertical dotted line with the liquidus line (the coordinates of this intersection point: 750 °C and 0.40 wt% Ti)

Equation 7 was obtained from fitting the liquidus in the Al-rich corner of the Al–Ti phase diagram [73] (see Fig. 11), coupled with the Gibbs energy of formation data of Al_3Ti [74] (see Table 1). The mathematical form of Eq. 7 is in agreement with thermodynamic constraints [89]. Equation 7 is in a reasonable agreement with experimental heat of mixing data [90]. At temperatures around the liquidus, Equation 7 is also in a reasonable agreement with previous Calphad assessments [58, 91, 92]. The almost vertical dotted line in Fig. 11 corresponds to the following equilibrium:

$$1/3\,\mathrm{Al_4C_3} + [\mathrm{Ti}] = \mathrm{TiC} + 4/3[\mathrm{Al}] \quad (8)$$

In agreement with reaction (8), the equilibrium Ti-content can be calculated as:

$$C_{\mathrm{Ti,cr}} \cong 100 \cdot \frac{M_{\mathrm{Ti}}}{M_{\mathrm{Al}}} \cdot \exp\left(\frac{\Delta_f G^{o}_{\mathrm{TiC}} - 0.333 \cdot \Delta_f G^{o}_{\mathrm{Al_4C_3}} - \Delta G^{E\infty}_{\mathrm{Ti(Al)}}}{R \cdot T}\right) \quad (9)$$

This equation is derived by supposing that the solubility of carbon in the Al–Ti liquid alloy is zero and that activity of Al in the alloy is close to 1. The critical Ti-content calculated by Eq. 9 increases from 0.40 wt% at 750 °C to 0.42 wt% at 900 °C. Based on Fig. 11, the "standard"

temperature of 800 °C is selected for our experiments. It is expected that at this T reaction (6) will be shifted to the right and the Al–Ti/C interface will be covered by TiC, supposing sufficient amount of Ti is added to the system through K_2TiF_6.

Appendix 6: The condition of perfect wettability

Now let us consider a liquid (L) metallic droplet on a solid surface (S) in the environment of a molten flux (F). The contact angle (Θ) of the droplet can be written by the Young equation applied to this case:

$$\cos\Theta = \frac{\sigma_{SF} - \sigma_{SL}}{\sigma_{LF}} \tag{10}$$

where σ_{SF}, σ_{SL}, and σ_{LF} are interfacial energies in solid/flux, solid/liquid metal, and liquid metal/flux systems, respectively. By definition, the adhesion energy in the solid/flux (W_{SF}) and in the solid/liquid metal (W_{SL}) can be written as:

$$W_{SF} = \sigma_{SG} + \sigma_{FG} - \sigma_{SF} \tag{11a}$$

$$W_{SL} = \sigma_{SG} + \sigma_{LG} - \sigma_{SL}, \tag{11b}$$

where σ_{SG}, σ_{LG}, and σ_{FG} are surface energy of the solid and surface tension of the liquid metal and molten flux, respectively. Let us express σ_{SF} and σ_{SL} from Eqs. 11a–b and substitute these values into Eq. 10:

$$\cos\Theta = \frac{(W_{SL} - \sigma_{LG}) - (W_{SF} - \sigma_{FG})}{\sigma_{LF}} \tag{12}$$

The condition of perfect wettability of S by L under F is that $\cos\Theta = 1$. Substituting this into Eq. 12, the critical W_{SL} value ensuring perfect wettability is obtained as:

$$W_{SL} \geq \sigma_{LF} + \sigma_{LG} + W_{SF} - \sigma_{FG} \tag{13}$$

On the other hand, adhesion energy in the S/L system can be modeled as a linear combination of adhesion energies along a heterogeneous solid/liquid interface. In the first approximation, let us suppose that some β_{TiC} fraction of the initial graphite (C) surface is covered by TiC. Then, the average adhesion energy is written as:

$$W_{SL} = W_{C/L} + \beta_{TiC} \cdot \left(W_{TiC/L} - W_{C/L}\right) \tag{14}$$

where $W_{C/L}$ and $W_{TiC/L}$ are the adhesion energies in graphite/liquid metal and TiC/liquid metal systems. As follows from Eq. 14, at $\beta_{TiC} = 0$: $W_{SL} = W_{C/L}$, while at $\beta_{TiC} = 1$: $W_{SL} = W_{TiC/L}$. Let us substitute Eq. 14 into Eq. 13 and let us express the critical value of $\beta_{TiC,cr}$ above which the contact angle becomes zero:

$$\beta_{TiC,cr} = \frac{\sigma_{LF} + \sigma_{LG} + W_{SF} - \sigma_{FG} - W_{C/L}}{W_{TiC/L} - W_{C/L}} \tag{15}$$

Perfect wettability of graphite by liquid Al under the molten flux can be achieved only if the value of $\beta_{Ti,cr} \leq 1$, as unity is the physical limit of surface coverage. In other words, perfect wettability will be achieved if $\beta_{Ti} \geq \beta_{Ti,cr}$. Now, let us estimate the value of $\beta_{Ti,cr}$ using Eq. 15. Let us perform this analysis supposing that Eq. 2 has been shifted to the right, and, as a result, sufficient Ti is dissolved in liquid Al to ensure the formation of at least some TiC, in accordance with Fig. 11. Thus, we consider the following composition of solution phases: L = Al–Ti alloy, F = (NaCl–KCl)–$KAlF_4$–K_3AlF_6 flux. The calculations will be performed for the "standard" temperature of 800 °C (see Appendix 5).

Surface tension of different pure molten salts is given in Table 5. One can see that in the F = (NaCl–KCl)–$KAlF_4$–K_3AlF_6 flux, the potassium salts are surface active. The estimated surface tension value is $\sigma_{FG} = 90 \pm 5$ mJ/m^2.

The contact angle of Na_3AlF_6 on a graphite surface is about 140° [76]. Combining this value with its surface tension (Table 5), and the Young equation, a value of solid/liquid interfacial energy of 272 mJ/m^2 is obtained (the solid/gas interfacial energy of graphite is taken as 150 mJ/m^2 [71]). From the contact angle of NaCl on C (113° [71]), the solid/liquid interfacial energy equals 195 mJ/m^2. Thus, among sodium salts, the chlorides are

Table 5 Surface tension of some liquid metals and molten salts ($\sigma = a + b \cdot t + c \cdot t^2$, σ in mJ/m^2, t in °C)

Pure component	a	b	c	σ at 800° C	Source
Al	1175	−0.19	–	1023	[38, 93–97]
Ti	1964	−0.25	–	1764	[97]
NaCl	171.5	−0.0719	–	114.0	[98]
KCl	160.4	−0.077	–	98.8	[98]
NaF	267.2	−0.082	–	201.6	[98]
KF	176.2	−0.0108	-0.333×10^{-4}	146.2	[98]
Na_3AlF_6	262.0	−0.128	–	159.6	[98]
K_3AlF_6	173	−0.059	–	126	Estimated[a]
$NaAlF_4$	210	−0.1	–	130	[76]
$KAlF_4$	139	−0.07	–	83	Estimated[a]

[a] Estimated from the values of Na_3AlF_6 and from the comparison of the NaCl–KCl and NaF–KF couples

interface active at the flux/graphite interface. Let us suppose that this is also the case for the potassium salts. Then, KCl will be segregated to the flux/graphite interface with an adhesion energy of $W_{SF} = 120 \pm 5$ mJ/m^2 [71].

As follows from Table 5, Ti is not surface active in liquid Al [93]. Thus, the following value is used here: $\sigma_{LG} = 1023 \pm 30$ mJ/m^2. This value corresponds to the nonoxidized surface of aluminum [38, 94–97].

(using $\sigma_{CG} = 150$ mJ/m^2 [71] and σ_{LG} values from Table 5) being equal to 1095 mJ/m^2 for the Al/C and to 1744 mJ/m^2 for the Ti/C interface. Thus, Ti in the Al–Ti alloy is not interface active at the C/L interface (in the absence of chemical interaction). Therefore, the $W_{C/Al}$ value is selected for $W_{C/L} = 78 \pm 15$ mJ/m^2.

Now, let us estimate the interfacial energies in the Al/TiC and Ti/TiC systems using the following equation [108]:

$$\sigma_{TiC/M} \cong \frac{0.195 \cdot f_{b,M}^{1/3} \cdot (\Delta_m H_{Ti} + \Delta_m H_C) + 0.216 \cdot \left(\Omega_{M-Ti} + \Omega_{M-C} - \Delta_f H^o_{TiC}\right) + 4.16 \cdot T}{(V_{TiC} \cdot V_M \cdot N_{Av})^{1/3}} \quad (17)$$

The interfacial energy in the (NaCl–KCl)/Al system with different additives was studied in [87, 99–102]. Using the experimental data and theories given in these papers, the estimated value for our system is found as: $\sigma_{LF} = 600 \pm 30$ mJ/m^2.

The adhesion energy in the nonreactive M/C system (M: liquid metal, C: covalent element) can be estimated from the London-van-der-Waals dispersion interaction [103, 104]. Taking into account also the repulsive term using the Lennard-Jones potential and dividing the resulting interaction energy by the average molar interface area, the adhesion energy is obtained with a negative sign as:

$$W_{C/M} \cong \frac{3}{4 \cdot f \cdot (V_M \cdot V_C \cdot N_{Av})^{1/3}} \cdot \frac{\alpha_M \cdot \alpha_C}{(R_M + R_C)^6} \cdot \frac{I_M \cdot I_C}{I_M + I_C} \pm 20\% \quad (16)$$

with $f = 1.0$, geometrical factor [97], V_i is the molar volume of component i (m^3/mol), N_{Av} is the Avogadro number (6.02×10^{23} L/mol), α_i is the polarizability of the gaseous atom i (m^3), R_i is radius of atom i (m), I_i is the first ionization energy of gaseous atom i (J/mol). The physical constants for carbon: $V_C = 5.3 \times 10^{-6}$ m^3/mol [105], $R_C = 1.85 \times 10^{-10}$ m [105], $I_C = 1.08 \times 10^6$ J/mol [105], and $\alpha_C = 1.76 \times 10^{-30}$ m^3 [106]. The physical constants for Al (and Ti): $V_M = 1.1 \times 10^{-5}$ (1.2×10^{-5}) m^3/mol [84], $R_M = 1.43 \times 10^{-10}$ (1.45×10^{-10}) m [105], $I_M = 5.77 \times 10^5$ (6.58×10^5) J/mol [105], $\alpha_M = 6.8 \times 10^{-30}$ (14.6×10^{-30}) m^3 [106]. Substituting these values into Eq. 16: $W_{C/Al} = 78 \pm 15$ mJ/m^2, $W_{C/Ti} = 170 \pm 34$ mJ/m^2. Using the Young-Dupre equation and Table 5, the contact angles are obtained as 157° and 154° in the Al/C and Ti/C systems, respectively. These values fit well into the data-bank on contact angles of nonreactive covalent/metallic couples [36, 37, 107]. From the definition of adhesion energy, the solid/liquid interfacial energies can be calculated

where $f_{b,M}$ is the bulk packing fraction of the solid metal M, $\Delta_m H_i$ is melting enthalpy of component i (J/mol), Ω_{i-j} is the interaction energy between components i and j of the liquid alloy in the approximation of the regular solution model (J/mol). Values of the general parameters: $\Delta_m H_{Ti} = 2.09 \times 10^4$ J/mol [105], $\Delta_m H_C = 1.05 \times 10^5$ J/mol [105], $\Delta_f H^o_{TiC} = -1.72 \times 10^5$ J/mol [74], $V_{TiC} = 1.4 \times 10^{-5}$ m^3/mol [109]. The parameter values for M = Al: $f_b = 0.74$, $V_{Al} = 1.1 \times 10^{-5}$ m^3/mol [84], $\Omega_{Al-Ti} = -6.6 \times 10^4$ J/mol (see Eq. 7), $\Omega_{Al-C} = -1.6 \times 10^4$ J/mol [58]. Then, the calculated value from Eq. 17: $\sigma_{TiC/Al} = 1020 \pm 200$ mJ/m^2. The parameter values for M = Ti: $f_b = 0.74$, $V_{Ti} = 1.2 \times 10^{-5}$ m^3/mol [84], $\Omega_{Ti-Ti} = 0$ (by definition), $\Omega_{Ti-C} = -1.8 \times 10^5$ J/mol [110]. Then, the calculated value from Eq. 17: $\sigma_{TiC/Ti} = 534 \pm 110$ mJ/m^2. As $\sigma_{TiC/Ti} < \sigma_{TiC/Al}$, Ti is an interface active component at the Al–Ti/TiC interface. Nevertheless, Ti is not able to decrease the interfacial energy of the Al–Ti/TiC interface significantly, due to its low solubility (see Fig. 11) and negative excess Gibbs energy (see Eq. 7). Thus, the requested value approximately equals: $\sigma_{TiC/L} = 1000 \pm 210$ mJ/m^2.

The adhesion energy $W_{TiC/L}$ can be calculated from its definition of Eq. 11b: $W_{TiC/L} = \sigma_{TiC/G} + \sigma_{L/G} - \sigma_{TiC/L}$. The surface energy of TiC is taken from [108]: $\sigma_{TiC/G} = 2250 \pm 250$ mJ/m^2. The surface tension of the liquid alloy was found above: $\sigma_{LG} = 1023 \pm 30$ mJ/m^2. The interfacial energy was estimated above: $\sigma_{TiC/Al} = 1000 \pm 210$ mJ/m^2. Then, the following result is obtained for the adhesion energy: $W_{TiC/L} = 2273 \pm 490$ mJ/m^2.

Finally, the critical TiC coverage of the C-surface ensuring perfect wettability is found from Eq. 15 as: $\beta_{TiC,cr} = 0.72 \pm 0.25$. Thus, the possible interval of values of $\beta_{TiC,cr}$ is between 0.47 … 0.97. Hence, one can expect that liquid Al will perfectly wet carbon under the given molten flux if about 72% of the carbon surface is covered by TiC. This theoretical result is in agreement with

experimental observation of [64] that liquid Al perfectly wets pure TiC under a fluoride flux.

Appendix 7: Mass balance requirements

Now, let us write the mass balance of Ti as follows:

$$m_{\mathrm{Ti}}^{\mathrm{in}} = m_{\mathrm{Ti}}^{\mathrm{Al}} + m_{\mathrm{Ti}}^{\mathrm{TiC}} + m_{\mathrm{Ti}}^{\mathrm{ox}} + m_{\mathrm{Ti}}^{\mathrm{loss}}, \quad (18)$$

where the masses of Ti (m_{Ti}, kg) mentioned in Eq. 18 correspond to the following items:

(i) the mass introduced into the system by the K_2TiF_6-content of the flux (in),
(ii) the mass dissolved in liquid Al (Al),
(iii) the mass bonded into TiC at the Al–Ti/C interface (TiC),
(iv) the mass spent to dissolve the oxide layer from the surface of the Al droplet (ox),
(v) the mass lost due to evaporation, etc. (loss).

Now, let us model shortly each item of Eq. 18. For this, let us consider the initial mass of the flux (m_{F}, kg), the initial mass of liquid Al (m_{Al}, kg), the initial surface area of carbon (A_{C}, m^2). The task is to make the full surface A_{C} wettable by liquid Al. The goal of this model is to find the critical condition of perfect wettability. Thus, all conditions will be taken at minimum values ensuring perfect wettability.

Let us denote the initial concentration of K_2TiF_6 in the salt by $C_{\mathrm{K_2TiF_6}}$ (wt%). Then, the mass of Ti introduced into the system by the K_2TiF_6-content of the flux is written as:

$$m_{\mathrm{Ti}}^{\mathrm{in}} = 2.0 \times 10^{-3} \cdot m_{\mathrm{F}} \cdot C_{\mathrm{K_2TiF_6}}, \quad (19)$$

where 2.0×10^{-3} is the ratio of molar masses of Ti to K_2TiF_6, divided by 100.

According to Fig. 11, about 0.406 wt% of Ti dissolved in liquid Al is needed to ensure stability of the TiC at the Al–Ti/C interface at 800 °C. Thus, the following equation describes the minimum required mass of Ti dissolved in liquid Al:

$$m_{\mathrm{Ti}}^{\mathrm{Al}} \geq 4.06 \times 10^{-3} \cdot m_{\mathrm{Al}} \quad (20)$$

If intermetallic particles Al_3Ti precipitate from liquid Al, the actual mass of Ti will be higher than that calculated by Eq. 20.

According to nanothermodynamics, there is a minimum thickness of phases above which they behave in a "macroscopic" way. Let us take this thickness of the TiC layer being equal to $\delta_{\mathrm{TiC,cr}} = 10\ \mathrm{nm} = 10^{-8}$ m. Let us suppose that this is the minimum thickness of the TiC layer, which is able to provide perfect wettability of C by Al–Ti. Then, the minimum required volume of TiC is calculated as: $V_{\mathrm{TiC}} = A_{\mathrm{C}} \cdot \delta_{\mathrm{TiC,cr}} \cdot \beta_{\mathrm{TiC,cr}}$. Multiplying this volume by the density of TiC (4280 $\mathrm{kg/m^3}$ [109]) and by the ratio of molar masses of Ti to TiC (0.80), the minimum mass of Ti, required in the TiC-bonded form to ensure perfect wettability is obtained as:

$$m_{\mathrm{Ti}}^{\mathrm{TiC}} \geq 2.5 \times 10^{-5} \cdot A_{\mathrm{C}} \quad (21)$$

In Eq. 21, $\beta_{\mathrm{TiC,cr}} = 0.72$ and $\delta_{\mathrm{TiC,cr}} = 10^{-8}$ m are involved. In reality, the thickness of the TiC layer might be above 10 nm, or the coverage of the carbon surface can also be higher than the critical coverage. In both cases, the actual mass of Ti will be higher than that calculated by Eq. 21. Comparing Eqs. 20 and 21, it is obvious that the amounts of Ti dissolved in liquid Al and that bonded in TiC become equal if 168 $\mathrm{m^2}$ of carbon is in contact with 1 kg of liquid Al.

Let us suppose that Al is used as ingots of side lengths $a * a * b$ with $b = 3 * a$. Then, taking into account the density of Al (2700 $\mathrm{kg/m^3}$ [105]), the surface area of Al is calculated as: $A_{\mathrm{Al}} = 0.035 \cdot m_{\mathrm{Al}}^{2/3}$. Let us suppose that this surface area is covered by a thin oxide layer of thickness δ_{ox}. Then, the total mass of Al_2O_3 introduced into the system in the form of an oxide layer is calculated as (taking into account the density of Al_2O_3 of 3900 $\mathrm{kg/m^3}$ [111]): $m_{\mathrm{ox}} = 137 \cdot \delta_{\mathrm{ox}} \cdot m_{\mathrm{Al}}^{2/3}$. As experiments show [49], chloride salts such as (NaCl–KCl) do not dissolve alumina. However, the solubility of alumina increases with increasing the concentration of fluorides. For simplicity, let us suppose that the solubility of alumina in the flux (C_{sol}) is proportional to the concentration of K_2TiF_6 in the flux: $C_{\mathrm{sol}} = 0.01 \cdot C^* \cdot C_{\mathrm{K_2TiF_6}}$ (with C^* being the solubility of alumina in pure K_2TiF_6). By definition, the solubility of alumina in the flux is expressed as: $C_{\mathrm{sol}} \equiv 100 \cdot m_{\mathrm{ox}}/m_{\mathrm{F}}$. From here, the amount of flux being able to dissolve the oxide can be written: $m_{\mathrm{F}}^{\mathrm{ox}} = 100 \cdot m_{\mathrm{ox}}/C_{\mathrm{sol}}$. Substituting into this equation, the above equations for m_{ox} and C_{sol}, the mass of flux needed to dissolve the oxide layer is found. From here, the mass of Ti within this flux can be calculated by an equation being analogous to Eq. 19: $m_{\mathrm{Ti}}^{\mathrm{ox}} = 2740 \cdot \frac{\delta_{\mathrm{ox}}}{C^*} \cdot m_{\mathrm{Al}}^{2/3}$. For simplicity we can write:

$$m_{\mathrm{Ti}}^{\mathrm{ox}} \cong k_{\mathrm{ox}} \cdot m_{\mathrm{Al}}^{2/3} \quad (22)$$

The thickness of the fresh oxide layer is about $\delta_{\mathrm{ox}} = 100$ nm. The value of C^* depends on temperature and composition of the salt (for a fixed equimolar (NaCl–KCl) salt it is constant at given T). In the first approximation, $C^* = 0.1$ wt%. Substituting these two approximated values into the above equation: $k_{\mathrm{ox}} \equiv 2740 \cdot \frac{\delta_{\mathrm{ox}}}{C^*} \cong 2.7 \times 10^{-3}$.

The loss of Ti is mainly due to its dissociation with the consequent evaporation of TiF_4 and oxidation by the surrounding gas. Under the given conditions, the mass of lost Ti is proportional to the concentration of K_2TiF_6 in the flux:

$$m_{\mathrm{Ti}}^{\mathrm{loss}} = k_{\mathrm{loss}} \cdot C_{\mathrm{K_2TiF_6}}. \quad (23)$$

The semi-empirical coefficient k_{loss} is a function of temperature, time, and other experimental conditions.

Now, let us substitute Eqs. 19–23 into Eq. 18:

$$2.0 \times 10^{-3} \cdot m_F \cdot C_{K_2TiF_6} \geq 4.06 \times 10^{-3} \cdot m_{Al} + 2.5 \times 10^{-5} \cdot A_C + k_{ox} \cdot m_{Al}^{2/3} + k_{loss} \cdot C_{K_2TiF_6} \quad (24)$$

From Eq. 24, the critical mass ratio of the flux to Al to ensure perfect wettability can be found as:

$$\frac{m_F}{m_{Al}} \geq \frac{1}{C_{K_2TiF_6}} \cdot \left(2.03 + 500 \cdot \frac{k_{ox}}{m_{Al}^{1/3}} + 0.0125 \cdot \frac{A_C}{m_{Al}}\right) + \frac{500 \cdot k_{loss}}{m_{Al}} \quad (25)$$

One can see that there are parameters with uncertain values (k_{ox}, k_{loss}) in Eq. 25. That is why an experimental program was performed to find the values of these semi-empirical parameters. The critical condition of perfect wettability of graphite by liquid Al under NaCl–KCl–K_2TiF_6 flux was measured and the results were compared to Eq. 25 in the main text of this paper (see Figs. 2–7).

When all parameters are fixed except the K_2TiF_6 concentration, Eq. 25 can be written in terms of the critical ratio $(m_F/m_{Al})_{cr}$ needed for perfect wettability as:

$$\left(\frac{m_F}{m_{Al}}\right)_{cr} = A + \frac{B}{C_{K_2TiF_6}} \quad (25a)$$

$$A = \frac{500 \cdot k_{loss}}{m_{Al}} \quad (25b)$$

$$B = 2.03 + 500 \cdot \frac{k_{ox}}{m_{Al}^{1/3}} + 0.0125 \cdot \frac{A_C}{m_{Al}} \quad (25c)$$

Thus, plotting the experimentally determined values of $(m_F/m_{Al})_{cr}$ as function of $1/C_{K_2TiF_6}$, the semi-empirical parameters A and B can be found by a linear fit in accordance with Eq. 25a. Using Eqs. 25b and c, the values of k_{loss} and k_{ox} can be evaluated if m_{Al} and A_C are known.

References

1. Li D, Li D, Zhang X, Sun T, Yao G (2010) J Alloys Comps 489:L1
2. Klinter AJ, Leon-Patino CA, Drew RAL (2010) Acta Mater 58:1350
3. Calderon NR, Voytovich R, Narciso J, Eustathopoulos N (2010) J Mater Sci 45:2150. doi:10.1007/s10853-009-3909-6
4. Barzilai S, Lomberg M, Aizenshtein M, Froumin N, Frage N (2010) J Mater Sci 45:2085. doi:10.1007/s10853-009-4018-2
5. Koltsov A, Crisci A, Hodaj F, Eustathopoulos N (2010) J Mater Sci 45:2062. doi:10.1007/s10853-009-4066-7
6. Drevet B, Pajani O, Eustathopoulos N (2010) Solar Energy Mater Solar Cells 94:425
7. Schmitz J, Brillo J, Egry I (2010) J Mater Sci 45:2144. doi:10.1007/s10853-010-4212-2
8. Kozlova O, Voytovich R, Protsenko P, Eustathopoulos N (2010) J Mater Sci 45:2099. doi:10.1007/s10853-009-3924-7
9. Budai I, Kaptay G (2010) J Mater Sci 45:2090. doi:10.1007/s10853-009-3907-8
10. Plevachuk Yu, Hoyer W, Kaban I, Köhler M, Novakovic R (2010) J Mater Sci 45:2051. doi:10.1007/s10853-009-4120-5
11. Klinter AJ, Leon CA, Drew RAL (2010) J Mater Sci 45:2174. doi:10.1007/s10853-009-4056-9
12. Kozlova O, Braccini M, Voytovich R, Eustathopoulos N, Martinetti P, Devismes M-F (2010) Acta Mater 58:1252
13. Israel R, Voytovich R, Protsenko P, Drevet B, Camel D, Eustathopoulos N (2010) J Mater Sci 45:2210. doi:10.1007/s10853-009-3889-6
14. Kaptay G, Bárczy T (2005) J Mater Sci 40:2531. doi:10.1007/s10853-005-1987-7
15. Kaptay G (2008) Comp Sci Technol 68:228
16. Verezub O, Kálazi Z, Buza G, Verezub NV, Kaptay G (2009) Surf Coat Technol 203:3049
17. Kaptay G (2006) Coll Surf A 282–283:387
18. Budai I, Kaptay G (2009) Metall Mater Trans A 40A:1524
19. Morita M, Baba H (1973) J Japan Inst Metals 37:315
20. Goddard DM, Burke PD, Kizer DE, Bacon R, Harrigan WC (1987) In: Engineered materials handbook, vol 1, Composites. ASM, USA, pp 867–873
21. Xia Z, Mao Z, Zhou Y (1991) Z Metallkund 82:766
22. Vidal-Setif MH, Lancin M, Marhic C, Valle R, Raviart JL, Daux JC, Rabinovits M (1999) Mater Sci Eng A272:321
23. Pippel E, Woltersdorf J, Doktor M, Blucher J, Degisher HP (2000) J Mater Sci 35:2279. doi:10.1023/A:1004787112162
24. Blucher JT, Narusawa U, Katsumata M, Nemeth A (2001) Composites A 32:1759
25. Etter T, Papakyriacou M, Schulz P, Uggowitzer PJ (2003) Carbon 41:1017
26. Kainer KU (2003) Metal matrix composites. Wiley-VCH, Weinheim, p 314
27. Blucher JT, Dobranszky J, Narusawa U (2004) Mater Sci Eng A387–389:867
28. Liu Z, Zhang G, Li H, Sun J, Ren M (2005) Mater Design 26:83
29. Rodriguez A, Sanchez SA, Narciso J, Louis E, Rodriguez-Reinoso F (2005) J Mater Sci 40:2519. doi:10.1007/s10853-005-1985-9
30. Wang TC, Fan TX, Zhang D, Zhang GD (2005) Mater Trans 46:1741
31. Rodriguez-Guerrero A, Sanchez SA, Narciso J, Louis E, Rodriguez-Reinoso F (2006) Acta Mater 54:1821
32. Flores-Zamora MI, Estrada-Guel I, Gonzalez-Hernandez J, Miki-Yoshida M, Amrtinez-Sanchez R (2007) J Alloy Comp 434–435:518
33. Tang Y, Huang Z, Liu Y, Liu L, Hu W (2008) Int J Mater Res 99:222
34. Orbulov IN, Németh A, Dobránszky J (2008) Mater Sci Forum 589:137
35. Tjong SC (2009) Carbon nanotube reinforced composites. Wiley-VCH, Berlin, p 228
36. Eustathopoulos N, Joud JC, Desre P (1974) J Mater Sci 9:1233. doi:10.1007/BF00551836
37. Naidich IV, Chuvashov IN, Ishuk NF, Krasovskii VP (1983) Poroshk Metal 6:67
38. Kaptay G (1991) Mater Sci Forum 77:315
39. Weirauch DA, Balaba WM, Perrotta AJ (1995) J Mater Res 10:640
40. Landry K, Kalogeropoulou S, Eustathopoulos N (1998) Mater Sci Eng 254:99

41. Eustathopoulos N, Nicholas MG, Drevet B (1999) Wettability at high temperatures. Pergamon, Amsterdam, p 420
42. Rocher JP, Quenisset JM, Naslan R (1989) J Mater Sci 24:2697. doi:10.1007/BF02385613
43. Kaptay G, Báder E, Bolyán L (2000) Mater Sci Forum 329–330:151
44. Nakae H, Yamamoto K, Sato K (1991) Mater Trans JIM 32:531
45. Rajan TPD, Pillai RM, Pai BC (1998) J Mater Sci 33:3491. doi:10.1023/A:1004674822751
46. Rams J, Ureña A, Escalera MD, Sánchez M (2007) Composites A 38:566
47. Ureña A, Rams J, Escalera MD, Sánchez M (2007) Composites A 38:1947
48. Masson B, Taghei MM (1989) Mater Trans JIM 30:411
49. Roy RR, Sahai Y (1997) Mater Trans JIM 38:995
50. Choh T, Kammel R, Oki T (1987) Z Metallkund 78:286
51. Kennedy AR, Karantzalis AE (1999) Mater Sci Eng A 264:122
52. Zhuxian Q, Mingjie Z, Yaxin Y, Zhenghan C, Grjotheim SK, Kvande H (1988) Aluminium 64:606
53. Zhuxian Q, Yaxin Y, Mingjie Z, Grjotheim SK, Kvande H (1988) Aluminium 64:1254
54. Lee MS, Terry BS, Grieveson P (1993) Metall Trans 24B:955
55. Jarfors A, Fredriksson H (1991) Mater Sci Eng A125:119
56. Svendsen L, Jarfors A (1993) Mater Sci Technol 9:948
57. Viala JC, Peillon N, Lochefert L, Bouix J (1995) Mater Sci Eng A203:222
58. Frage N, Frumin N, Levin L, Polak M, Dariel MP (1998) Metall Mater Trans 29A:1341
59. Jarfors AEW (1999) Mater Sci Technol 15:481
60. Kennedy AR, Weston DP, Jones MI (2001) Mater Sci Eng A316:32
61. Frumin N, Frage N, Polak M, Dariel MP (1997) Scripta Mater 37:1263
62. Contreras A, Leon CA, Drew RAL, Bedolla E (2003) Scripta Mater 48:1625
63. Contreras A, Bedolla E, Perez R (2004) Acta Mater 52:985
64. Lopez VH, Kennedy AR (2006) J Colloid Interface Sci 298:356
65. Tepliakov FK, Oskolskich AP, Kaluzhskii NA, Shusterov VS, Ivchenko VP (1991) Cvetnie Metall 9:54
66. Lee MS, Terry BS, Grieveson P (1993) Metall Trans 24B:947
67. El-Mahallawy N, Taha MA, Jarfors AEW, Fredriksson H (1999) J Alloy Comp 292:221
68. Murty BS, Kori SA, Chakraborty M (2002) Int Mater Rev 47:3
69. Birol Y (2006) J Alloys Comp 420:207
70. Birol Y (2008) J Alloys Comp 454:110
71. Baumli P, Kaptay G (2008) Mater Sci Eng A495:192
72. Smirnov MV (1973) Electrode potentials in molten chlorides. Nauka, Moscow, p 244 (in Russian)
73. Massalski TB (1990) Binary alloy phase diagrams, 2nd edn. ASM International, Materials Park, OH
74. Barin I (1993) Thermochemical properties of pure substances. VCh, New York
75. Chase MW (1985) J Phys Chem Data 14:731
76. Grjotheim K, Krohn C, Malinovsky C, Matiasovsky K, Thonstad J (1982) Aluminium electrolysis, 2nd edn. Aluminium-Verlag, Düsseldorf
77. Lee MS, Terry BS, Grieveson P (1994) Trans Inst Min Metall 103:C26
78. Chernov RV, Ermolenko IM (1973) Zh Neorg Himii 18:1372
79. Posipaiko VI, Alekseeva EA (1977) Phase diagram of molten salts, Part 2. Metallurgiia, Moscow (in Russian)
80. Chernov RV, Ermolenko NM (1970) Zh Neorg Himii 15:1962
81. Buhalova GA, Maslennikova GN, Rabkin DM (1962) Zh Neorg Himii 7:1640
82. Malcev VT, Buhalova GA (1965) Zh Neorg Himii 10:1464
83. Kobalev FV, Ioffe VM, Karcev VE (1970) Zh Neorg Himii 15:1211
84. Iida T, Guthrie RIL (1993) The physical properties of liquid metals. Clarendon Press, Oxford, p 288
85. Janz GJ, Dampier FW, Lakshminarayanan GR, Lorentz PK, Tomkins RPT (1968) Molten slats: volume 1, electrical conductance, density and viscosity data. NSRDS-NBS 15, Washington, USA, 139 pp
86. Danek V, Matiasovsky K (1989) Z Anorg Allg Chem 570:184
87. Martin-Garin L, Dinet A, Hicter JM (1979) J Mater Sci 14:2366. doi:10.1007/BF00737025
88. Roy RR, Ye J, Sahai Y (1997) Mater Trans JIM 38:566
89. Kaptay G (2004) Calphad 28:115
90. Esin IO, Bobrov NI, Petrushevskii MS, Geld PV (1974) Metalli 5:104
91. Kaufman L, Nesor H (1978) Calphad 2:325
92. Ansara I, Dinsdale AT, Rand MH (1998) Thermochemical database for light metal alloys, COST 507, vol 2. EUR18499 EN, Belgium
93. Keene BJ (1993) Int Mater Rev 38:157
94. Goumiri L, Joud JC (1982) Acta Metal 30:1397
95. Garcia-Cordovilla C, Louis E, Pamies A (1986) J Mater Sci 21:2787. doi:10.1007/BF00551490
96. Sarou-Kanian V, Millot F, Rifflet JFC (2003) Int J Thermophys 24:277
97. Kaptay G (2008) Mater Sci Eng A495:19
98. Janz GJ, Lakshminarayanan GR, Tomkins RPT, Wong J (1969) Molten slats: volume 2, section 2. Surface tension data, NSRDS-NBS 28, Washington, USA, pp 49–111
99. Silny A, Utigard TA (1996) J Chem Eng Data 41:1340
100. Ye J, Sahai Y (1996) Mater Trans JIM 37:1479
101. Roy RR, Sahai Y (1997) Mater Trans JIM 38:546
102. Roy RR, Utigard TA (1998) Metall Mater Trans 29B:821
103. Atkins PW (1990) Physical chemistry, 4th edn. University Press, Oxford
104. Kaptay G (2003) Interfacial forces, energies and phenomena. DSc thesis, Miskolc, Hungary
105. Emsley J (1989) The elements. Clarendon Press, Oxford
106. Lide DR (1993–1994) CRC handbook of chemistry and physics. CRC Press, Boca Raton
107. Kumar G, Pranbu KN (2007) Adv Colloid Interface Sci 133:61
108. Kaptay G (2005) Mater Sci Forum 473–474:1
109. Kosolapova TYa (1986) Properties, synthesis and application of refractory compounds. Metallurgiia, Moscow (in Russian)
110. Frisk K (2003) Calphad 27:367
111. Samsonov GV (1978) Physico-chemical properties of oxides. Metallurgiia, Moscow (in Russian)